The inertial subrange in turbulent pipe flow: centre line.

J. F. MORRISON[1]†, **M. VALLIKIVI**[2] **and A. J. SMITS**[2,3]

[1]Department of Aeronautics, Imperial College, London SW7 2AZ, UK

[2]Department of Mechanical & Aerospace Engineering, Princeton University, Princeton NJ 08544, USA

[3]Department of Mechanical & Aerospace Engineering, Monash University, VIC 3800, Australia

(Received 28 November 2015)

The inertial subrange scaling of the axial velocity component is examined for the centre line of turbulent pipe flow for Reynolds numbers in the range $249 \leqslant Re_\lambda \leqslant 986$. Estimates of the dissipation rate are made by both integration of the one-dimensional dissipation spectrum and the third-order moment of the structure function. In neither case does the non-dimensional dissipation rate asymptote to a constant; rather than decreasing, it increases indefinitely with Reynolds number. Complete similarity of the inertial range spectra is not evident: there is little support for K41, and effects of Reynolds number are not well represented by Kolmogorov's "extended similarity hypothesis", K62. The second-order moment of the structure function does not show a constant value, even when compensated by K62. When corrected for the effects of finite Reynolds number, the third-order moments of the structure function accurately support the "$\frac{4}{5}$ths" law, but they do not show a clear plateau. In common with recent work in grid turbulence, nonequilibrium effects can be represented by an heuristic scaling that includes a global Reynolds number as well as a local one. It is likely that nonequilibrium effects appear to be particular to the nature of the boundary conditions. Here, the principal effects of the boundary conditions appear through finite turbulent transport at the pipe centre line which constitutes a source or a sink at each wavenumber.

1. Introduction

The similarity hypotheses of Kolmogorov (1941*a*,*b*, here designated as K41) constitute one of the few cornerstones in the subject of turbulence. Even so, Kolmogorov (1962, here designated as K62) himself had to refine his theory of "universal equilibrium" (see also Obukhov 1962) in order to account for departures from local isotropy due to the effects of spatial fluctuations of the energy dissipation rate. While these papers are admirably concise in themselves, it is hardly surprising that they continue to be the subject of much interest: excellent summaries with historical perspectives are provided by Kraichnan (1974); Sreenivasan (1991); Sreenivasan & Antonia (1997), Ishihara *et al.* (2009) and Vassilicos (2015).

The consensus view of local isotropy is that it relies on a wide separation of scales in order that the energy-containing scales do not influence the small-scale dissipating eddies, other than through the mean dissipation rate, ϵ. What exactly constitutes a "wide" separation

† Email address for correspondence: j.morrison@imperial.ac.uk

of scales has been the subject of much debate and questions remain over the cause of high-wavenumber intermittency. A demonstration of a wide scale separation (but not necessarily of local isotropy) is the celebrated relationship attributed to Taylor (1935),

$$\epsilon = A_1 \frac{u^3}{l}, \tag{1.1}$$

where u and l are, respectively, the velocity scale and length scale of the energy-containing turbulence and A_1 is a constant. It is widely acknowledged (but not universally accepted - see Davidson 2004, p.77) that A_1 is a universal constant at asymptotically large Reynolds numbers. While the simulations of isotropic turbulence by Ishihara *et al.* (2009) show that A_1 asymptotes to a constant as the Taylor microscale Reynolds number, $Re_\lambda \rightarrow 1200$, they also show finite Reynolds number effects. The work of Vassilicos (2015) and colleagues has considered the nonequilibrium effects of initial and large-scale conditions.

(1.1) is an insufficient criterion for local isotropy because it is certainly the case that high-wavenumber intermittency increases with Reynolds number (or equivalently, with decreasing scale) as exemplified by the non-Gaussian behaviour of dissipation-related statistics. (See Batchelor & Townsend 1949). Yet, little is known about the origins of intermittency and whether it might be attributable to the effects of Reynolds number, mean shear or solid boundaries, or whether it is intrinsic to the Navier-Stokes equations themselves (Kraichnan 1974). Ishihara *et al.* (2009) illustrate the importance of internal shear layers that lead to intermittency. Nor is it straightforward to separate out the effects of boundary conditions. Moreover, these hypotheses rely almost exclusively on experimental validation which has always been limited by the relatively low Reynolds number available in most facilities. Sreenivasan & Antonia (1997) emphasised the need for detailed measurements at high Reynolds numbers ($Re_\lambda > 1000$) of inertial range statistics in representative shear flows for which the large scales are well defined.

The spectral form of K41 — as postulated by Obukhov (1962) — has received support from many experiments both in the atmosphere and in the ocean (see for example, Grant *et al.* 1962), both in the form of the inertial subrange law as well as the collapse of spectra exhibiting universal equilibrium. Yet, questions remain and laboratory experiments in a single facility in which the boundary conditions are well controlled are few. Using an inertial-subrange scaling that enables use of a linear ordinate, Saddoughi & Veeravalli (1994) were able to show that the inertial subrange and local isotropy do not necessarily coincide — see also Mestayer (1982). Of the two decades exhibiting a -5/3 slope on log-log axes, only the higher one had a spectral shear correlation coefficient approaching zero. Durbin & Speziale (1991) show that an assumption of local isotropy is not justified even at high Reynolds numbers if the mean strain rate is not small, as suggested by Lumley (1992). Bradshaw (1967) identified a "first-order" inertial subrange, for which a sufficient criterion is that energy sources or sinks are a small fraction of the spectral transfer. He identified $Re_\lambda > 100$ to be a sufficient criterion for a wide range of flows, both with and without shear.

Both K41 and K62 theories are cast in the form of moments of velocity differences, $(\Delta u_i)^n$, — since termed "structure functions" by Monin & Yaglom (1975) — so that, in the direction i, $\Delta u_i = u_i(x_i + \frac{r_i}{2}) - u_i(x_i - \frac{r_i}{2})$ for separation r_i. Dual studies are limited, notable exceptions in shear flows being Saddoughi & Veeravalli (1994); Mydlarski & Warhaft (1996), among others. Many of the ambiguities associated with the definition

of the $-5/3$ inertial subrange law might be clarified by appeal to a unifying physical process.

Here, we explore the development of the inertial subrange in pipe flow by examination of the behaviour of moments of the longitudinal velocity structure function, $\langle(\Delta u(r))^n\rangle$, for Reynolds numbers (based on pipe diameter and bulk mean velocity, $\overline{U}$) in the range, $2.5\times10^5 < Re_D < 6.0\times10^6$, that is for $249 \leqslant Re_\lambda \leqslant 986$ at the pipe centre line. For turbulent pipe flow, radius R, the revisions in K62 may be expressed as:

$$\frac{\langle(\Delta u(r))^n\rangle}{\upsilon_\epsilon^n} = C_n\left(\frac{r}{\eta}\right)^{n/3}\left(\frac{r}{R}\right)^{-\mu_n}, \tag{1.2}$$

for $\eta \ll r \ll R$, where $\eta = (\nu^3/\epsilon)^{\frac{1}{4}}$, is the Kolmogorov length scale, $\upsilon_\epsilon = (\nu\epsilon)^{\frac{1}{4}}$ the Kolmogorov velocity scale and ν the kinematic viscosity. The exponents, μ_n, and constants, C_n, are undetermined and therefore require experimental estimation. They are presumed universal although this is the source of some debate, see for example Sreenivasan & Antonia (1997) and Sreenivasan (1995). Here, μ_n is a measure of the deviation of the exponent from the locally-isotropic value, $n/3$, and increases with n. As might be expected, behaviour of the lower moments provides no information concerning the behaviour of the higher ones. Assuming a log-normal distribution for the dissipation averaged over a volume of linear dimension r, ϵ_r, K62 gives

$$\mu_n = \frac{1}{18}\mu n(n-3), \tag{1.3}$$

where μ is supposedly universal. Its physical significance is illustrated by the sixth-order moment where the dissipation rate correlated over r is proportional to

$$\langle(\Delta u(r))^6\rangle \sim \left(\frac{R}{r}\right)^{\mu}. \tag{1.4}$$

As $\mu > 0$ always, (1.4) expresses the increase in the spatial intermittency with Reynolds number or equivalently, a reduction in scale. Monin & Yaglom (1975) suggest $\mu \approx 0.4 - 0.5$. They also provide the Fourier space equivalent to (1.2) as:

$$\phi_{11}(k_1) = C\epsilon_r^{\frac{2}{3}}k_1^{-\frac{5}{3}}(k_1R)^{-\frac{\mu}{9}}. \tag{1.5}$$

At the centre line, the transport equation for the turbulence kinetic energy reduces to

$$-\frac{1}{\zeta}\frac{d}{d\zeta}\left[\zeta\left(\frac{1}{2}\overline{q^2v} + \frac{\overline{p'v}}{\rho}\right)\right] = \epsilon, \tag{1.6}$$

where $\zeta = R - y$ and in which the pressure transport term is the much smaller one of the two. At the centre line of fully developed pipe flow (no streamwise gradients), axisymmetry forces to zero radial gradients of even-order products only.

Scale-by-scale energy transfer is described by the Kármán-Howarth-Monin equation (Monin & Yaglom 1975; Frisch 1995) for the second-order structure function. Assuming stationary, homogeneous (but not isotropic) fully developed flow at the pipe centre line,

it reduces to a balance between inertial energy transfer, viscous diffusion and dissipation (Marati *et al.* 2004). With the assumption of local isotropy, integration yields Kolmogorov's equation:

$$-\langle(\Delta u)^3\rangle + 6\nu\frac{d}{dr}\langle(\Delta u)^2\rangle = \frac{4}{5}\epsilon r. \tag{1.7}$$

In the inertial subrange, the viscous term may be assumed to be negligible (Saddoughi & Veeravalli 1994; Antonia *et al.* 1997; Antonia & Burattini 2006) and Kolmogorov's $\frac{4}{5}$ths law is obtained:

$$\langle(\Delta u)^3\rangle = -\frac{4}{5}\epsilon r. \tag{1.8}$$

Hence, in addition to the dissipation rate, an isotropic estimate of the enstrophy may be of interest.

(1.6) also indicates that exact isotropy cannot be consistent with stationarity at any Reynolds number because the turbulent transport in (1.6) appears in the spectral budget as a source or a sink at each wavenumber. This makes the case for a close examination of the additional spectral transfer arising through scale inhomogeneity (Lumley 1967). Antonia *et al.* (1997) show that $\epsilon_{iso}/\epsilon \approx 0.95$ for simulated channel flow at low Reynolds number ($Re_\tau = 395$). Therefore, in the present measurements at much higher Reynolds numbers, we take the $\frac{4}{5}$ths law as a reasonably accurate estimate of centre-line disspation rate. Danaila *et al.* (2001) have proposed a generalized form of Kolmogorov's equation to account for the effects of large scale transport in fully developed channel flow appearing through the left-hand side of (1.6). However, the additional term involves the longitudinal structure function for the wall normal fluctuations.

2. Experimental techniques

Measurements were performed in the Princeton/ONR Superpipe using NSTAP probes of length, $\ell = 30$ μm or 60 μm, with temporal resolution up to 300 kHz. The datasets from which the present results derive ($250 \times 10^3 \leqslant Re_D \leqslant 6.0 \times 10^6$) are those previously reported by Vallikivi *et al.* (2011); Rosenberg *et al.* (2013); Hultmark *et al.* (2013); Vallikivi (2014). Structure functions (up to third-order moments) and spectra are calculated using time series of either 60 s or 90 s duration: the latter have previously been presented by Rosenberg *et al.* (2013), and their scaling at lower wavenumbers examined by Vallikivi *et al.* (2015). Full details of the experiments appear in Vallikivi (2014).

Dissipation spectra (see Rosenberg *et al.* 2013, figure 3) show two decades of inertial subrange. All data conform to the criterion for a "first-order" subrange proposed by Bradshaw (1967), $Re_\lambda > 100$. Note that all spectra extend beyond both the noise floor and the viscous cut-off. An isotropic estimate of ϵ is calculated by integration of the dissipation spectra,

$$\epsilon_{iso} = 15\nu\int_0^\infty k_1^2\phi(k_1)dk_1, \tag{2.1}$$

up to the frequency at which the noise floor is determined and taken to be the minimum of the spectral estimate. At the highest Reynolds number, $Re_D = 6 \times 10^6$, the Kolmogorov length scale, $\eta \approx 10$ μm, equivalent to $l = 3\eta$, or $k_1\eta|_{max} \approx 2$: note that the dissipation spectrum peaks at $k_1\eta \approx 0.1$. See table 1. Inspection of the spectra shows that, at

Case	Re_D	Re_τ	Re_λ	$\langle U \rangle$ [m/s]	$\frac{\nu}{u_\tau}$ [μm]	ℓ^+	ℓ/η	ϵ_{iso} [m^2/s^3]	ϵ [m^2/s^3]	λ [mm]	
1	247×10^3	5,412	249	8.40	12	5.0	0.57	1.19	0.682	3.29	+
2	512×10^3	10,481	338	9.37	6.2	9.7	0.96	1.37	0.852	2.27	○
3	1.1×10^6	20,250	457	10.5	3.2	18.8	1.61	1.65	1.11	1.57	□
4	2.1×10^6	37,690	610	10.5	1.7	35.0	2.64	1.43	1.05	1.10	not plotted
5	2.1×10^6	37,690	564	10.5	1.7	17.4	1.31	1.41	1.02	1.07	△
6	4.0×10^6	68,371	785	10.3	0.95	31.7	2.14	1.44	0.966	0.773	×
7	6.0×10^6	98,190	986	10.6	0.66	45.5	2.97	1.77	1.14	0.625	▽

TABLE 1. Experimental conditions of NSTAP measurements at pipe flow centre line. ϵ_{iso} is estimated using (2.1). ϵ, η and Re_λ are estimated using (1.8).

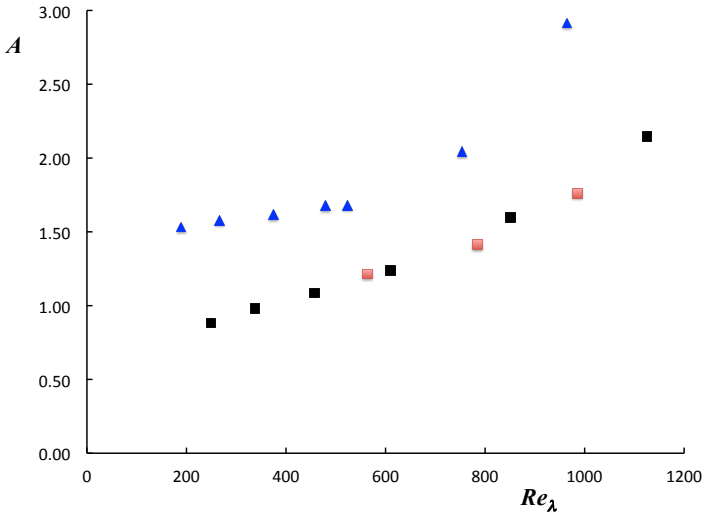

FIGURE 1. Nondimensional dissipation rate, $A = \epsilon R/u_\tau^3$. ▲, isotropic dissipation estimate, (2.1); ■, "4/5ths" law, (1.8).

$Re_D = 6 \times 10^6$, the noise floor appears at $k_1\eta \approx 0.5$; at $Re_D = 4 \times 10^6$, it appears at $k_1\eta \approx 0.7$. Therefore it is likely that the spectra at the two highest Reynolds numbers are slightly under-resolved, suggesting that the estimate of dissipation is likely to be low. Vallikivi (2014) estimates the errors associated with the spectral estimates of the dissipation rate in the range of 2% to 16% increasing with Reynolds number. It is probably for this reason that ϵ does not converge to the value of ϵ_{iso} as Reynolds number increases.

3. Results

Analysis comprises a first and second pass: the first provides estimates of the first three moments through time-averaging of velocity differences. The third moment is then used

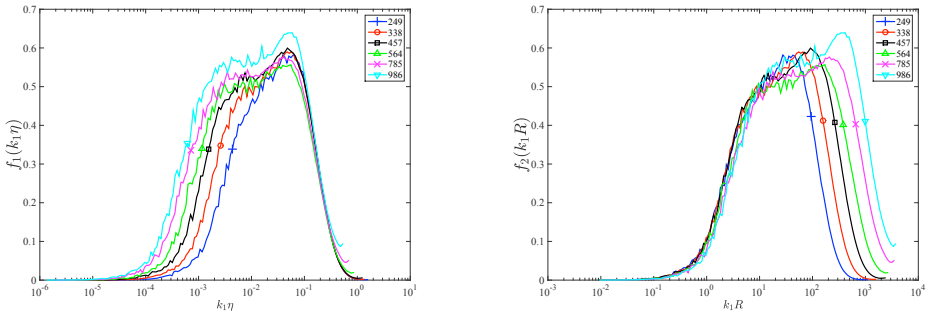

(a) Inner scaling (b) Outer scaling

FIGURE 2. Premultipled subrange spectra, $f_1(k_1\eta)$, (3.1) and $f_2(k_1R)$, (3.2).

to calculate estimates of the dissipation rate using (1.8). The second pass is used to calculate probability density functions for the velocity differences and their moments up to arbitrary order. In what follows, for consistency, scaling of spectra is performed using dissipation rate estimates using (2.1) while scaling of structure functions is performed using estimates of dissipation rate from (1.8).

Figure 1 shows A plotted as a function of Re_λ, where $\epsilon = v_\epsilon^3/\eta = Au_\tau^3/R$. Here, ϵ estimated using (1.8) is taken to be the maximum over a range of r/η — this is made necessary by the nature of the third-order moments which do not show a pronounced plateau, as shown below. It is noticeable that neither dissipation estimate provides values of A that asymptote to a constant: rather A increases almost linearly with Re_λ. The ordinate is proportional to the estimate ϵ: therefore the increase in A at higher Reynolds numbers cannot be attributed to poor spatial resolution. Furthermore, there is a remarkable consistency between estimates of A using (1.8) obtained using the 30 μm and 60 μm probes.

3.1. *K41*

Figure 2 shows compensated inertial-subrange spectra where $k_1 = 2\pi f/U$ is the streamwise wavenumber and U is the local streamwise mean velocity. With inner, viscous scaling:

$$f_1(k_1\eta) = \epsilon^{-\frac{2}{3}} k_1^{\frac{5}{3}} \phi_{11}(k_1) = \frac{(k_1\eta)^{\frac{5}{3}}}{v_\epsilon^2} \phi_{11}(k_1\eta) \tag{3.1}$$

and with outer scaling:

$$f_2(k_1R) = \epsilon^{-\frac{2}{3}} k_1^{\frac{5}{3}} \phi_{11}(k_1) = A^{-\frac{2}{3}} \frac{(k_1R)^{\frac{5}{3}}}{u_\tau^2} \phi_{11}(k_1R). \tag{3.2}$$

At sufficiently large Reynolds number, classical subrange scaling gives $f_1(k_1\eta) \to C$ and $f_2(k_1R) \to C$ where $C \approx 0.5$ (Monin & Yaglom 1975). While f_1 collapses at high wavenumbers and f_2 collapses at low wavenumbers, there is no clear classical inertial subrange scaling. Rather, both scalings suggest a more shallow slope than $-5/3$: Vallikivi *et al.* (2015) have previously reported that the inertial subrange slope is closer to $-3/2$ than $-5/3$. Interestingly, the simulations of isotropic turbulence by Ishihara *et al.* (2009) suggest a steeper spectral slope of $-5/3 + \mu$ where $\mu \approx -0.1$. Both sets of spectra in

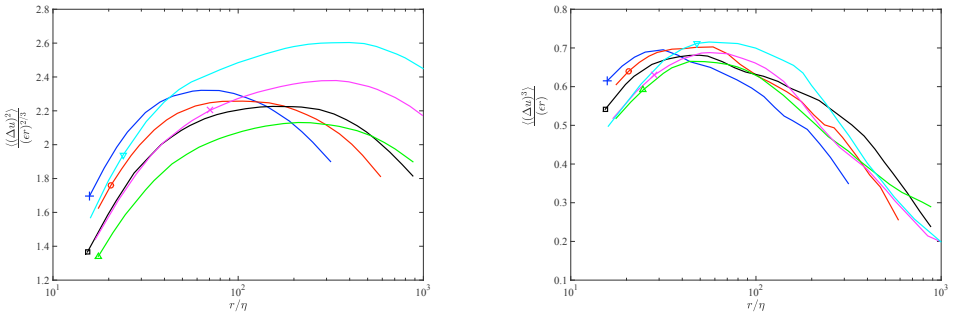

(a) Second-order ($n = 2$) moments, C_2 (b) Third-order ($n = 3$) moments, C_3

FIGURE 3. Second- and third-order structure functions: C_2, C_3. $\zeta_n = n/3, \mu_n = 0$.

figure 2 show a 'spectral bump' at $k_1\eta \approx 0.05$ that could correspond to the "bottleneck phenomenon" (Falkovich 1994) - energy transfer arising from the viscous suppression of triadic interactions due to the rapid roll-off of the energy spectrum in the dissipation range. This phenomenon has also been shown by Saddoughi & Veeravalli (1994) and McKeon & Morrison (2007) at similar wavenumbers: however, it is difficult to discuss sensibly without first demonstrating a self-similar inertial subrange.

Figure 3 shows second and third-order structure functions: no smoothing over a range of values of r is used. With increasing Reynolds number, both moments are characterised by a reduction in the ordinate value at small r/η followed by increasing ordinate values at large r/η. This gives the appearance of each plot line being rotated anti-clockwise as the Reynolds number increases. For the second-order moment, K41 suggests that $C_2 \approx 2.0$ in the inertial range (say, $30 \lesssim r/\eta \lesssim 200$): figure 3a indicates that the constant is Reynolds-number dependent, even for $Re_\lambda > 500$. In figure 3b, we expect a plateau in the inertial range, which in the limit of very large Reynolds number will asymptote to a constant of 4/5 given by (1.8). However, no clear plateau is evident; instead a peak appears around $r/\eta \approx 60$. Using a correction for finite Reynolds number ($C_3 = 0.8 - 8.45 Re_\lambda^{-2/3}$, Lundgren 2002), a plateau value of 0.80 ± 0.01 is obtained for the three highest Reynolds numbers.

3.2. *K62*

With the inclusion of the effects of spatial intermittency, the appropriate spectral form of (1.5) when compensated becomes

$$g_1(k_1\eta) = (k_1R)^{\frac{\mu}{9}}\, f_1(k_1\eta), \quad g_2(k_1R) = (k_1R)^{\frac{\mu}{9}}\, f_2(k_1R), \qquad (3.3a,b)$$

for, respectively, inner and outer scalings. These are equivalent to the K41 scalings of (3.1) and (3.2). (See Monin & Yaglom 1975, p. 642, for example). Figure 4 shows spectra in this form, $\mu = 0.5$. Comparison of figures 2(a) and 4(a) shows that the degree of collapse with inner scaling is generally worse with the K62 compensation. Similarly, comparison of figures 2(b) and 4(b) shows that the degree of collapse is approximately the same, but the slope on the inertial range has increased.

The nature of the incomplete similarity illustrated by figures 4 (a,b) may be further

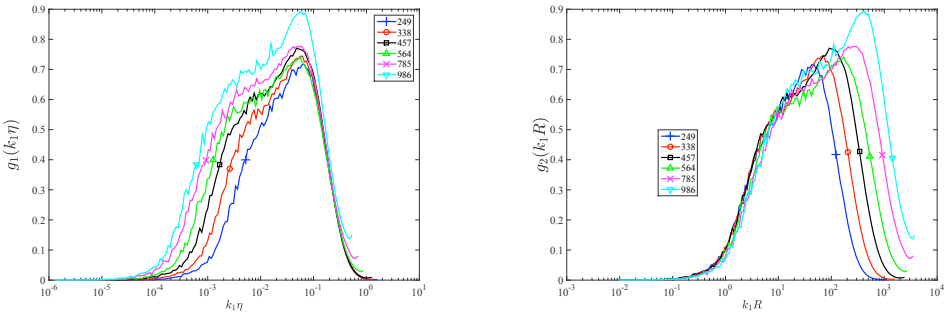

(a) Inner scaling (b) Outer scaling

FIGURE 4. Premultipled subrange spectra, K62 scaling: inner scaling $g_1(k_1\eta)$, (3.3a); outer scaling $g_2(k_1R)$, (3.3b). $\mu = 0.5$. Same data as those in figure 2.

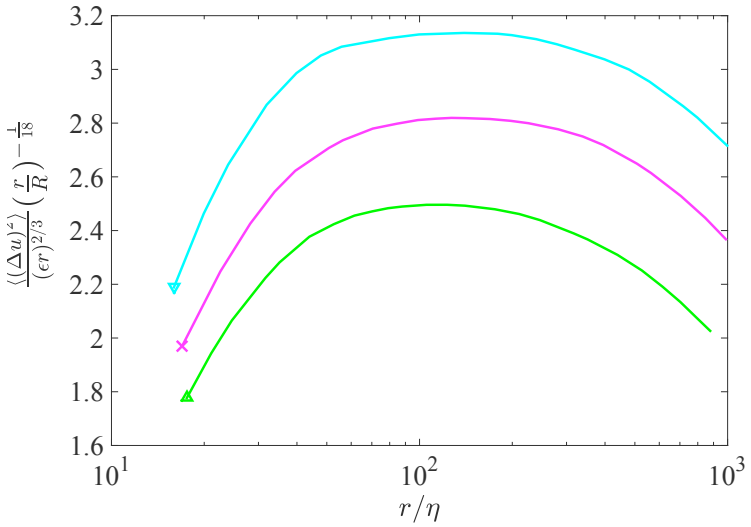

FIGURE 5. Second-order ($n = 2$) moments, compensated for K62, (1.2) $\mu = 0.5$.

investigated by examining the second-order structure function (the third-order moments are unchanged). Figure 5 shows the second-order structure function corrected for the effects of large-scale intermittency using (1.2) with $n = 2$ and $\mu = 0.5$. Although it shows a broad plateau (its width increasing with Reynolds number), C_2 shows an even greater Reynolds-number dependence than the corresponding K41 scaling, figure 3(a).

4. Discussion

We believe the results of figure 1 to be our most far reaching. It is important to note that the nondimensionalisation of ϵ here uses the imposed scales u_τ and R, rather than the more usual nondimensionalisation using "intrinsic" scales, such as the rms of the fluctu-

ating velocity $u' = \sqrt{\overline{u^2}}$, and the dissipation lengthscale $L_\epsilon = u'^3/\epsilon$, (see, for example, Sreenivasan 1995; Ishihara *et al.* 2009). Trivially, one could write $B = \epsilon/(u'^3/L_\epsilon) \equiv 1$. Therefore the use of imposed scales in figure 1 describes non self-similar effects of the boundary conditions on the spectral flux, here caused by large scale transport.

Hultmark *et al.* (2012) show that, at the centre line, $u'^+ = u'/u_\tau$ is more or less constant with Reynolds number. Writing

$$A = \epsilon/(u_\tau^3/R) = \frac{u'^3/L_\epsilon}{u_\tau^3/R} \sim R/L_\epsilon, \tag{4.1}$$

the slight increase of A with Re_λ can be interpreted as the influence of the outer boundary condition on ϵ: by using the locally isotropic estimate, $\epsilon = 15\nu\overline{(\frac{\partial u}{\partial x})^2} \sim u_\tau^3/R$,

$$A = \epsilon/(u_\tau^3/R) = 15R^+/Re_\lambda^2 \sim 1. \tag{4.2}$$

Hence (4.2) does not fully account for the effects of the outer boundary condition in spite of assuming $\epsilon \sim u_\tau^3/R$. This important result is not the same as that shown, for example, by Sreenivasan (1995), in which the influence of the large scales appears as $C_\epsilon \equiv A$ **decreasing** with Re_λ. Vassilicos (2015) has suggested that for turbulence grids, "Inlet, I" or global effects may be accounted for $C_\epsilon \sim Re_I^m/Re_L^n$ with $m \approx 1 \approx n$, where the subscript L denotes a local Reynolds number. This can be adapted for the present case by inspection so that (4.2) gives A increasing with Re_λ. Note that the formulation of K62 is such that ϵ retains its self-similar form, and that it therefore cannot describe the above effects.

The lack of a universal description of the inertial subrange suggests that an empirical approach might prove beneficial. Mydlarski & Warhaft (1996) present a modified similarity form in which (3.1) becomes

$$f_1^*(k_1\eta) = \epsilon^{-\frac{2}{3}} k_1^{\frac{5}{3}} \, (k_1\eta)^{-\frac{5}{3}+n_1} \, \phi_{11}(k_1) = \frac{(k_1\eta)^{n_1}}{v_\epsilon^2}\phi_{11}(k_1\eta) \tag{4.3}$$

where n_1 is determined empirically using grid turbulence as

$$n_1 = \frac{5}{3}\big(1 - 3.15Re_\lambda^{-\frac{2}{3}}\big) \tag{4.4}$$

in the range $50 \leqslant Re_\lambda \leqslant 473$. At sufficiently large Reynolds number, $f_1^*(k_1\eta) \to C$. With outer scaling (4.3) becomes

$$f_2^*(k_1R) = A^{-\frac{2}{3}} \frac{(k_1R)^{n_1}}{u_\tau^2} \left(\frac{\eta}{R}\right)^{-\frac{5}{3}+n_1} \phi_{11}(k_1R), \tag{4.5}$$

where, at large Reynolds number, $f_2^*(k_1R) \to C$ also. Here the constant, μ of K62, (1.3) is replaced by the empirical function, (4.4).

Figures 6 (a,b) show spectra with inner and outer scalings indicated by (4.3) and (4.5) respectively: there are identifiable plateaux with both inner and outer scaling at the three highest Reynolds numbers, with an ordinate value of about 0.73, very close to the Mydlarski & Warhaft (1996) value. However, this is not the self-similar value of about 0.55 (see figure 2) and the difference is presumably due to the empirical function.

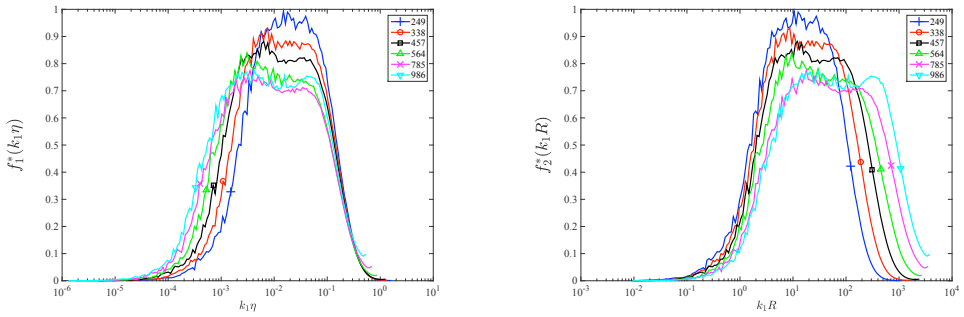

(a) Inner scaling (b) Outer scaling

FIGURE 6. Premultipled subrange spectra. Scaling exponent $k_1^{n_1}$, (4.4). Same data as figure 1.

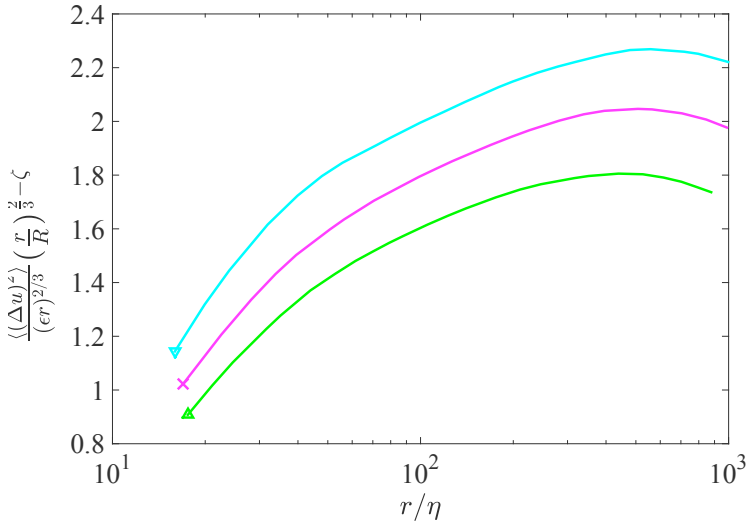

FIGURE 7. Second-order ($n = 2$) moments, compensated using Mydlarski & Warhaft (1996) function (4.4). Same data as figure 5.

The second-order structure function (the Fourier transform pair of 4.3) may be written

$$\frac{\left\langle(\Delta u)^2\right\rangle}{(\epsilon r)^{2/3}} = C_2\left(\frac{r}{R}\right)^{\zeta-\frac{2}{3}}, \tag{4.6}$$

where $\zeta = \frac{2}{3}\left(1 - 7.88Re_\lambda^{-2/3}\right)$, from (4.4). Figure 7 shows the second-order moment premultiplied to preserve the value of the constant C_2. In comparison to the K62 scaling in figure 5, the collapse is rather better. However, there is no clear plateau. The lack of collapse in both figures 6 and in figure 7 is perhaps not unexpected, given that the empirical information derives from decaying turbulence, rather than that at the centre line of fully developed pipe flow.

5. Conclusions

A dual space spectral description of energy flux has been provided for the centre line of turbulent pipe flow up to $Re_\lambda \approx 1000$. Direct effects of viscosity appear at the centre line although the correction of the "4/5ths" constant for finite Reynolds number by Lundgren (2002) yields values of 0.80 ± 0.01. It should be pointed out however, that Lundgren's theory is developed for decaying isotropic turbulence. A greater challenge is presented by the effects of transport, even at the centre line - Danaila *et al.* (2001) (see also Antonia & Burattini 2006) have investigated the need for corrections to (1.7) at low Reynolds numbers to account for the effects of the large scales. There is no clear plateau in the third-order moment even when corrected for the effects of boundary conditions as described by K62, or empirically. Both viscous and turbulent transport contribute to a non-conservative spectral flux, the effect of which is clearly evident in both the corresponding spectra and in the dimensionless dissipation rate. Turbulent transport, which is finite at the centre line (left hand side of 1.6), is clearly the dominant mechanism in determining global effects on spectral flux. Moreover, these effects cannot be described well by K62 in which ϵ retains its self-similar form.

Future work involves an investigation of the effects of mean shear, and examination of long data records to investigate high wavenumber intermittency.

This work was supported by the Office of Naval Research Grant No. N00014-13-1-0174. M.V. is grateful for additional financial support from Estonian Students Fund, Zonta International, as well as several Princeton alumni fellowships. J.F.M. is indebted to the Engineering and Physical Sciences Research Council (grants GR/M64536/01 and GR/R48193/01), an Engineering Foresight Award (Royal Academy of Engineering, England), and the Leverhulme Trust (grant F/07058/H) for financial support.

REFERENCES

Antonia, R. A. & Burattini, P. 2006 Approach to the 4/5 law in homogeneous isotropic turbulence. *J. Fluid Mech.* **550**, 175–184.

Antonia, R. A., Zhou, T. & Romano, G. P. 1997 Second- and third-order longitudinal velocity structure functions in fully developed turbulent channel flow. *Phys. Fluids* **9**, 3465–3471.

Batchelor, G. K. & Townsend, A. A. 1949 The nature of turbulent motion at large wavenumbers. *Proc. R. Soc. Lond. A* **199**, 238–255.

Bradshaw, P. 1967 Conditions for the existence of an inertial subrange in turbulent flow. Aero. 1220. Natl. Phys. Lab.

Danaila, L., Anselmat, F., Zhou, T. & Antonia, R. A. 2001 Turbulent energy scale budget equations in a fully developed channel flow. *J. Fluid Mech.* **430**, 87–109.

Davidson, P. A. 2004 *Turbulence. An Introduction for Scientists and Engineers*. Oxford University Press.

Durbin, P. & Speziale, C. G. 1991 Local anisotropy in strained turbulence at high Reynolds numbers. *J. Fluids Engng.* **113**, 707–709.

Falkovich, G. 1994 Bottleneck phenomenon in developed turbulence. *Phys. Fluids* **6**, 1411–1414.

Frisch, U. 1995 *Turbulence: The Legacy of A.N. Kolmogorov.*. Cambridge University Press.

Grant, H. L., Stewart, R. W. & Moillet, A. 1962 Turbulence spectra from a tidal channel. *J. Fluid Mech.* **12**, 241–268.

Hultmark, M., Vallikivi, M., Bailey, S. C. C. & Smits, A. J. 2012 Turbulent pipe flow at extreme Reynolds numbers. *Physical Review Letters* **108** (9), 1–5.

Hultmark, M., Vallikivi, M., Bailey, S. C. C. & Smits, A. J. 2013 Logarithmic scaling of turbulence in smooth- and rough-wall pipe flow. *J. Fluid Mech.* **728**, 376–395.

Ishihara, T., Gotoh, T. & Kaneda, Y. 2009 Study of high-Reynolds number isotropic turbulence by direct numerical simulation. *Ann. Rev. Fluid Mech.* **41**, 165–180.

Kolmogorov, A. N. 1941*a* Dissipation of energy in the locally isotropic turbulence. *Dokl. Akad. Nauk SSSR* **32**, 16–18, for English translation see: *Proc. R. Soc. Lond.* A **434**, 15–17.

Kolmogorov, A. N. 1941*b* The local structure of turbulence in incompressible viscous fluid with very large Reynolds numbers. *Dokl. Akad. Nauk SSSR* **30**, 301–305, for English translation see: *Proc. R. Soc. Lond.* A **434**, 9–13.

Kolmogorov, A. N. 1962 A refinement of previous hypotheses concerning the local structure of turbulence in a viscous incompressible fluid at high Reynolds number. *J. Fluid Mech.* **13**, 82–85.

Kraichnan, R. H. 1974 On Kolmogorov's inertial-range theories. *J. Fluid Mech.* **62**, 305–330.

Lumley, J. L. 1967 The inertial subrange in nonequilibrium turbulence. In *Atmospheric Turbulence and Radio Wave Propagation* (ed. A. M. Yaglom & V. I. Tatarski), pp. 157–165. Moscow: Nauka Press.

Lumley, J. L. 1992 Some comments on turbulence. *Phys. Fluids A* **4**, 203–211.

Lundgren, T. S. 2002 Kolmogorov two-thirds law by matched asymptotic expansion. *Phys Fluids* **14**, 638–642.

Marati, N., Casciola, C. M. & Piva, R. 2004 Energy casacade and spatial fluxes in wall turbulence. *J. Fluid Mech.* **521**, 191–215.

McKeon, B. J. & Morrison, J. F. 2007 Asymptotic scaling in turbulent pipe flow. *Phil. Trans. R. Soc. A* **365**, 771–787.

Mestayer, P. G. 1982 Local isotropy and anisotropy in a high-Reynolds-number turbulent boundary layer. *J. Fluid Mech.* **125**, 475–503.

Monin, A. S. & Yaglom, A. M. 1975 *Statistical Fluid Mechanics: Mechanics of Turbulence. Vol. II*. MIT Press.

Mydlarski, L. & Warhaft, Z. 1996 On the onset of high-Reynolds-number grid-generated wind tunnel turbulence. *J. Fluid Mech.* **320**, 331–368.

Obukhov, A. M. 1962 Some specific features of atmospheric turbulence. *J. Fluid Mech.* **13**, 77–81.

Rosenberg, B. J., Hultmark, M., Vallikivi, M. & Smits, A. J. 2013 Turbulence spectra in smooth- and rough-wall pipe flow at extreme Reynolds numbers. *J. Fluid Mech.* **731**, 46–63.

Saddoughi, S. G. & Veeravalli, S. V. 1994 Local isotropy in turbulent boundary layers at high Reynolds number. *J. Fluid Mech.* **268**, 333–372.

Sreenivasan, K. R. 1991 On local isotropy of passive scalars in turbulent shear flows. *Proc. R. Soc. Lond. A* **434**, 165–182.

Sreenivasan, K. R. 1995 On the universality of the Kolmogorov constant. *Phys. Fluids* **7**, 2778–2784.

Sreenivasan, K. R. & Antonia, R. A. 1997 The phenomenology of small-scale turbulence. *Ann. Rev. Fluid Mech.* **29**, 435–472.

Taylor, G. I. 1935 Statistical theory of turbulence. Part I. *Proc. R. Soc. Lond. A* **151**, 421–444.

Vallikivi, M. 2014 Wall-bounded turbulence at high Reynolds numbers. PhD thesis, Princeton University.

Vallikivi, M., Ganapathisubramani, B. & Smits, A. J. 2015 Spectral scaling in boundary layers and pipes at very high Reynolds numbers. *J. Fluid Mech.* **771**, 303–326.

Vallikivi, M., Hultmark, M., Bailey, S. C. C. & Smits, A. J. 2011 Turbulence measurements in pipe flow using a nano-scale thermal anemometry probe. *Expts. Fluids* **51**, 1521–1527.

Vassilicos, J. C. 2015 Dissipation in turbulent flows. *Ann. Rev. Fluid Mech.* **47**, 95–114.